The DC response of electrically conducting fractures excited by a grounded current source

Chester J Weiss, David F Aldridge, Hunter A Knox, Kimberly A Schramm, Sandia National Laboratories and Lewis C Bartel, Carbo Ceramics Inc.*

SUMMARY

We investigate through numerical simulation the usefulness of DC resistivity data for characterizing subsurface fractures with elevated electrical conductivity by considering a geophysical experiment consisting of a grounded current source deployed in a steel cased borehole. In doing so, the borehole casing behaves electrically as a spatially extended line source, efficiently energizing the fractures with a steady current. Finite element simulations of this experiment for a horizontal well intersecting a small set of vertical fractures indicate that the fractures manifest electrically in (at least) two ways: a local perturbation in the electric potential proximal the fracture set, with limited far–field expression; and, an overall reduction in the electric potential along the entire length of borehole casing due to enhanced current flow through the fractures into the surrounding formation. The change in casing potential results in a measureable effect that can be observed far from fractures themselves, at distances where the local perturbations in the electric potential around the fractures are imperceptible. Under these conditions, our results suggest that far–field, time–lapse measurements of DC potentials surrounding a borehole casing can be reasonably interpreted by simple, linear inversion for a Coulomb charge distribution along the borehole path, including a local charge perturbation due to the fractures. Such an approach offers an inexpensive method for detecting and monitoring the time-evolution of electrically conducting fractures while ultimately providing an estimate of their effective conductivity — the latter providing an important measure independent of seismic methods on fracture shape, size, and hydraulic connectivity.

INTRODUCTION

Mapping fluid flow in fractures is a long–standing geophysics problem central to energy resource exploration, groundwater management and assessment, waste disposal and monitoring contaminant transport. However, detailed geophysical mapping of individual fractures is complicated by their intrinsically multi-scale structure, with the finest details therein at length scales typically below the resolution limits of exploration-scale geophysical methods such as seismics or electromagnetics. In the context of energy exploration, one strategy for mapping fractures has been to monitor microseismicity associated with pumping or injection activities and invert for hypocenter location (House, 1987; Phillips et al., 1998), however, the relationship between hypocenter location and fracture genesis is not necessarily straightforward (e.g. Taftia et al., 2013) and can be confounded by low–impedance flow paths along existing fractures and reactivation of previously unmapped faults (Rutledge and Phillips, 2003).

A complementary strategy for mapping fractures is to sense the presence of electrically conductive fluids or materials within the fracture using electrical/electromagnetic geophysical methods, and monitor either the static or time-lapse evolution of fracture conductivity (Wright et al., 1985; Wills et al., 1992; Pribnow et al., 2003; Wilt and Morea, 2004). Recent thinking on the enhancement of fracture conductivity through injection of engineered fluids and materials has been aimed at hydrocarbon production (Cramer et al., 2010; Eick et al., 2011; Cannan et al., 2014) and there has been a commensurate increase in research activity on geophysical methods for detecting these electrically enhanced fracture systems within the context of borehole logging (Pardo and Torres-Verdín, 2012, 2013; Yang et al., 2013), cross–borehole electromagnetic imaging (Heagy et al., 2014b) and borehole–to–surface electromagnetic imaging (Hibbs, 2014; Cannan et al., 2014)

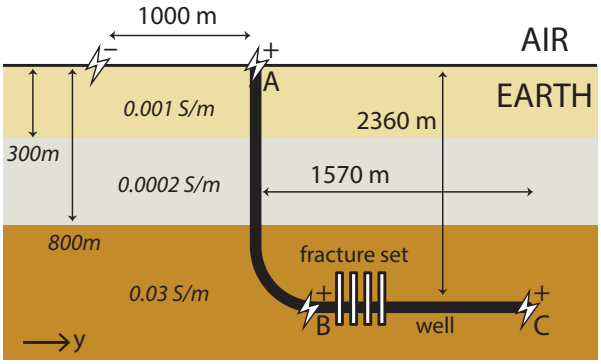

Figure 1: Cross section of an idealized petroleum production scenario showing a short stack of conductive, vertical fractures intersected by a horizontal well embedded in a three-layer geologic model. The system is energized by a pair of DC current electrodes (symbols): a negative pole located 1000 m away from the well head; and, a positive pole located down hole at one of three locations (A, B or C).

Inversion of electromagnetic data for fracture geometry is well–known to be problematic, especially with regularization geared toward smoothness (e.g. Constable et al., 1987). Recent success has been realized by imposing rigid geometric constraints (Robinson et al., 2013; Heagy et al., 2014a) and, instead, inverting for electrical conductivity with a predetermined fracture volume. Some theoretical work has been aimed at understanding how fractures (or more generally, any self-affine geologic system) lead to anomalous diffusion of electromagnetic fields (Everett, 2009; Ge et al., 2012, 2013) and fluid flow (Reeves et al., 2008a,b), which in turn, may lead to compact power-law parametrizations of the intrinsically complex fracture structure. Yet another approach is to invert for elements of the rank–2 electrical conductivity tensor and interpret its principal axes in terms of the fracture network orientation (e.g. Kriegshauser et al., 2002).

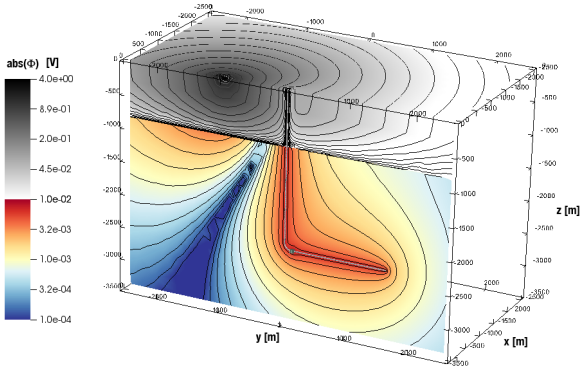

Figure 2: Oblique view of the magnitude of electric potential (in Volts) for case A (Figure 3) along two intersecting surfaces: a vertical slice at $x = 0$ m through the well track and fracture set; and, a horizontal slice at $z = 0$ m along the air/Earth interface (Figure 5, left). Intersecting the slices are the well track and fractures. Note the local perturbation near the well heel due to the fractures, as well as the dominance of the –1 A current source on the potentials at $z = 0$. Generally small amplitudes of the potential in the region below $z = -800$ m are consistent with its relatively high 0.03 S/m conductivity – in contrast to the low (< 0.001 S/m) conductivity in the region above $z = -800$ m.

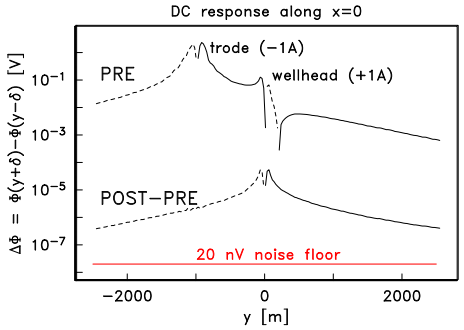

Figure 3: (top curve) Potential difference along line $x = 0$ directly through the well head and over the horizontal section of the well, in the absence of conducting fractures for 1 A source located at the well head (case A) and –1 A source at $y = -1000$ m. Dashed lines indicate negative values; solid lines, positive. (bottom curve) Scattered potential differences arising from a 10 S/m fracture set near the heel of the well bore. Potential differences computed using 100 m electrode separation, $\delta = 50$ m. For reference, also shown is the 20 nV noise floor for the 32-bit ZEN receiver from Zonge Engineering (http://zonge.com/instruments-home/systems/distributed-em-systems/).

In this study we numerically simulate a borehole–to–surface electromagnetic experiment (Bevc and Morrison, 1991; Tseng et al., 1998; Pardo et al., 2008b) in the zero–frequency limit of direct-current (DC) that is aimed at detection of a small set of vertical, electrically conductive fractures, intersecting the borehole. In particular, we focus on the scattered (or 'secondary') electric potential associated with differences in fracture conductivity from that of the background geology.

THEORY

We develop, test and use for analysis of the fracture system a finite element method for solving the DC resistivity problem of exploration geophysics. Specifically, for a 3D distribution of isotropic electrical conductivity σ excited by a time–invariant source current density $\mathbf{J}_s$ the electric scalar potential Φ is described by the solution to the well-known equation

$$-\nabla\cdot(\sigma\nabla\Phi) = \nabla\cdot\mathbf{J}_s, \tag{1}$$

where the 'positive' sign convention for electric field $\mathbf{E} = \nabla\Phi$ is assumed. A numerical solution to Eq (1) is derived over the finite spatial domain Ω which includes the conducting earth (with a potentially irregular topography) and source current $\mathbf{J}_s$, but excludes the air layer under the assumption of air being a perfect resistor. Therefore, at the air/earth interface Γ_N the normal derivative of Φ is set identically zero as a Neumann boundary condition in accordance with continuity of normal electric current at material interfaces and absence of surface currents. Furthermore, the side and lower boundaries Γ_D are taken sufficiently distant from area of interest within the model and thereby endowed, out of convenience, with a homogeneous (vanishing) Dirichlet boundary condition. Discretization of Eq (1) with a piecewise linear, nodal basis over tetrahedral elements results in a linear system of equations of the form

$$\mathbf{A}\mathbf{x} = \mathbf{b}. \tag{2}$$

Because the coefficient matrix $\mathbf{A}$ is symmetric positive definite, the linear system is solved iteratively in double precision using the conjugate gradient method (Hestenes and Stiefel, 1952) with Jacobi preconditioning and Polak and Ribière (1969) updates to mitigate potentially poor convergence from round-off error at each iteration. Although scalar finite element solutions such as the one just described are not particularly gluttonous in their consumption of compute resources, a matrix–free paradigm is adopted here whereby the action of the coefficient matrix $\mathbf{A}$ is computed element-wise by reconstructing the coefficients as needed rather than retrieving their stored values from deep computer memory (e.g. Weiss, 2001).

FRACTURE DETECTION SCENARIOS

We consider a generic production–well geometry of a horizontal wellbore embedded in a deep, electrically–conducting bed, overlain by resistive geology (Figure 1) – a scenario found in hydrocarbon and geothermal reservoirs (e.g. Pribnow et al., 2003; Pollastro et al., 2013) – whereby a negative DC current electrode is located on Earth's surface far from the wellhead and a positive DC current electrode is grounded on the well casing itself, either at the wellhead or some distance down hole. For simplicity, the amplitude of source current density $\mathbf{J}_s$ is taken as 1 A/m^2. Values of the potential for alterna-

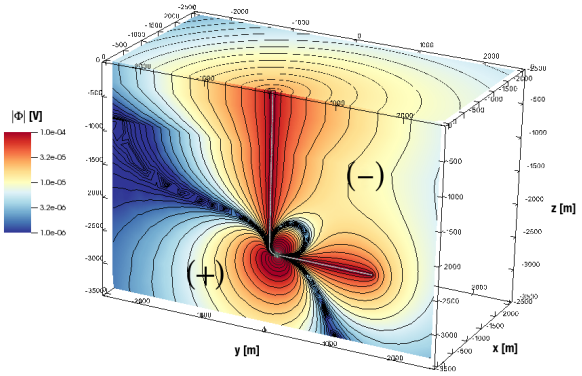

Figure 4: Oblique view of the magnitude of POST–PRE scattered electric potential for case A (Figure 1) along two intersecting surfaces: a vertical slice through the well track and fracture set at $x = 0$ m; and, a horizontal slice along the air/Earth interface $z = 0$ m (Figure 5, left). Region where $\Phi > 0$ is denoted by $(+)$ whereas the region $\Phi < 0$ is denoted by $(-)$. Superimposed on the slices is well bore and fractures. Note that this POST–PRE difference data arises from a combination of sources – one due to the conductivity perturbation at the fractures, and the other a change in the relative potential of the borehole casing due to current leakage at the fracture. Clearly, the scattered potential plotted here is due to currents outside of the region of the conductivity perturbation encapsulated by the local fracture geometry.

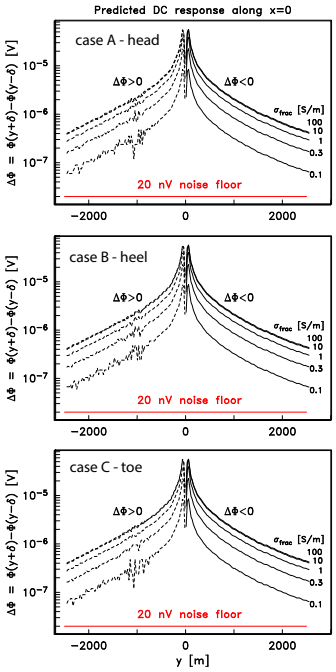

Figure 5: Scattered potential differences ($\delta = 50$ m) as a function of fracture conductivity over the range 0.1–100 S/m for a –1 A source at $y = -1000$ m and +1 A source located at either the well head, heel, or toe (cases A-C in Figure 1). Dashed lines indicate negative values; solid lines, positive.

tive source currents with magnitude k are simply those presented here, scaled by a factor k by the linearity of Eq. (1) in the source. For ease of analysis and comparison with previously published work (Heagy et al., 2014b), a short sequence of four electrically conductive fractures (each a short, thin, vertical slab $5 \times 60 \times 100$ m and separated by 15 m on center) are located 10 m from the start of the horizontal section of the wellbore. We note that, theoretically, the unstructured finite element mesh can accommodate realistic borehole and fracture geometries (Pardo et al., 2008a). However, for the large problem size under consideration here and an assumption that measurements of the potential (differences) will occur on Earth's surface, far from the fractures, there is little observable difference in the computed response of a 10 m diameter borehole and that of a smaller one with an equivalent volume-averaged conductivity. We take as the conductivity of the solid wellbore volume the value 10000 S/m, a rough estimate of the volume-averaged conductivity of a steel well casing with a fluid–filled interior. Lastly, we note that the 5 m "thickness" of each fracture is also artificially inflated, consistent with Heagy et al. (2014b), to avoid excessive mesh discretization and constraining our analysis to a particular microscale fracture model. Instead, we consider a range of bulk, volume–averaged conductivities for the rock/fracture/fluid system which span a likely range of values.

For evaluation of the Earth model (Figure 1) in terms of source current locations (A-C) and fracture conductivity, it is convenient to consider the model response in the absence of fractures and the response when fractures are present. We refer to such model results as "PRE" and "POST", respectively, out of reference to a hypothetical time–lapse survey where fractures are filled with a conductive material. Accordingly we define the 'scattered' response as the POST minus PRE difference.

Surface estimates on the Air/Earth interface of the electric potential from configuration A, where the borehole is energized with a +1 A current source at the wellhead show the expected potential distribution dominated by the unshielded -1 A current source at $y = -1000$ m, with a localized perturbation due the well head (Figure 2). Although these calculations of the potential distribution are useful for illuminating the physics of the DC resistivity problem, real-world DC resistivity data consist of potential differences measured between two distinct (electrode) points. As such, we take a nominal electrode separation of 100 m and estimate the predicted PRE and scattered data on a measurement profile parallel to and directly above the horizontal section of the well track (Figure 3). Amplitude estimates for these data are measurable with commercial instrumentation, however, high quality scattered data near the -1 A source may require recording at 24- or 32-bit word length because of the small differences between large PRE and POST values at that location. Evidenced in the potential difference data is a scattered signature centered on the well head with a gentle asymmetry reflecting the horizontal section of the well track and fracture response (Figure 4). The amplitude of this scattered response is a function of fracture conductivity (Figure 5), with high–conductivity fractures resulting in a large–amplitude response. Note that the magnitude of the response

is not proportional to the conductivity difference between the fractures and the 0.03 S/m background conductivity. Rather, as this conductivity difference increases, the scattered potential (differences) asymptote to a maximal value. Furthermore, consistent with the fact that the 10000 S/m borehole is roughly an equipotential surface, the scattered potential (difference) for scenarios B and C (where the +1 A source is located at the well heel and toe, respectively) is effectively equivalent with scenario A (Figure 5).

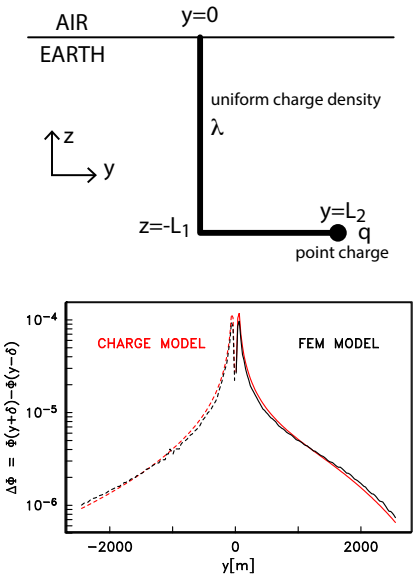

Figure 6: Interpretation (right) of POST–PRE response for toe-frac model $\sigma_{\text{frac}} = 10$ S/m (Figure 9) in terms of a uniform negative line charge density $\lambda = Q/(L_1 + L_2)$ along a simple well track, neglecting curvature at the heel, with an additional (positive) charge $-q$ at the toe, $y = 1500$ m (left). Model parameters used in this example are $Q = -2.2 \times 10^{-11}$ C and $q = 0.75Q = 1.65 \times 10^{-11}$ C.

One factor that does affect the scattered response is the location of the fracture set. Considering a +1 A source grounded at the wellhead, as before, but with fractures located at the well toe, one finds a measurably different scattered response with a pronounced asymmetry over the horizontal section of well (Figure 6). Noting that in the previous models, the scattered potential was the result, mainly, of a uniform negative charge distribution along the wellbore with a local net–positive charge in the vicinity of the fracture (Figure 5), we construct an approximate analytic model for interpreting this behavior, consisting simply of a uniform "L-shaped" distribution of negative electric charge superposed with a point positive charge at the fracture site (Figure 6). Reasonable agreement is achieved between results of this simple analytic model and those provided by the 3D finite element analysis (Figure 6, right), thus suggesting a possible mode for characterization of conducting fractures with DC resistivity data: where the effective charges Q and q are interpreted via rock physics in terms of fracture conductivity, morphology and distribution.

CONCLUSIONS

We present a finite element analysis of electromagnetic fields in the DC limit arising from conductive vertical fractures in a deep horizontal well that have been illuminated by a grounded well casing. The analysis suggests that the DC response of the fractures is measureable with commercially available EM instrumentation and that that signals arise largely from electrostatic loss along the well casing due to enhanced DC current leakage at the fracture site. The magnitude of these losses is a direct indicator of the effective electrical conductivity of fracture/fluid/rock system and hence they offer an independent constraint for fracture characterization.

We show that in a complicated arrangement of layered geology penetrated by a deviated borehole and compact 3D fracture sets, the DC resistivity results are largely independent of the location on the well casing at which the current source is grounded. This results suggest a field operational procedure whereby electrically conducting fractures can be detected and characterized with surface measurements of electric potential differences by simply energizing the well casing at the head, rather than though a complicated (and comparatively expensive) down-hole grounding instrument.

Lastly, we observe that scattered potentials directly computed by the finite element analysis possess at least two interesting properties. The first of which is that as fracture conductivity increases to large values, the scattered response asymptotes to a limiting value rather than scaling proportionally to the difference between fracture and background conductivity. This suggests that current loss through the fractures is bounded by some maximum value, likely to be geometrically constrained in some way, for infinite fracture conductivity. The second observation of note concerns the distribution of scattered potentials. We have shown that the "sources" $\nabla \cdot \mathbf{J}_s^{scat}$ which give rise to scattered potentials lie both at the fracture location and distributed along the length of the borehole. However, only the first of these sources is actually associated with a conductivity perturbation. Hence, even for mild conductivity perturbations (the usual assumption of Born Approximation Theory), coupling with the metal borehole casing is a significant source of scattered potential. And because the magnitude of the charge distribution $\nabla \cdot \mathbf{J}_s^{scat}$ is a function of fracture conductivity, it's conceivable to use continuous-time monitoring of surface potential measurements as an indicator of fracture genesis and maturation.

ACKNOWLEDGMENTS

The authors would like to thank Dr. Alex Rinehart for expertise in finite element meshing using CUBIT (cubit.sandia.gov). Funding for this work was provided by CARBO Ceramics, Inc., under CRADA agreement SC11/01780.00. Sandia National Laboratories is a multi-program laboratory managed and operated by Sandia Corporation, a wholly owned subsidiary of Lockheed Martin Corporation, for the U.S. Department of Energy's National Nuclear Security Administration under contract DE-AC04-94AL85000.

REFERENCES

Bevc, D., and H. F. Morrison, 1991, Borehole-to-surface electrical resistivity monitoring of a salt water injection experiment: Geophysics, **56**, 769–777.

Cannan, C., L. Bartel, T. Palisch, and D. F. Aldridge, 2014, Electrically conductive proppant and methods for detecting, locating and characterizing the electrically conductive proppant. (US Patent App. 14/147,372).

Constable, S. C., R. L. Parker, and C. G. Constable, 1987, Occam's inversion: A practical algorithm for generating smooth models from electromagnetic sounding data: Geophysics, **52**, 289–300.

Cramer, P., P. Eick, and J. Brewer, 2010, Controlled source fracture monitoring. (US Patent App. 12/621,789).

Eick, P. M., J. D. Brewer, and F. D. Janiszewski, 2011, Fracture detection via self-potential methods with an electrically reactive proppant. (US Patent App. 13/327,985).

Everett, M. E., 2009, Transient electromagnetic response of a loop source over a rough geological medium: Geophysical Journal International, **177**, 421–429. (doi: 10.1111/j.1365-246X.2008.04011.x).

Ge, J., M. E. Everett, and C. J. Weiss, 2012, Fractional diffusion analysis of the electromagnetic field in fractured media Part I: 2D approach: Geophysics, **77**, WB213–WB218.

———, 2013, 3D modeling of fractional diffusion to describe electromagnetic induction in fractured geological media: SEG Technical Program Expanded Abstracts, 1858–1862.

Heagy, L. J., A. R. Cockett, and D. W. Oldenburg, 2014a, Parametrized inversion framework for proppant volume in a hydraulically fractured reservoir: SEG Technical Program Expanded Abstracts, 865–869.

Heagy, L. J., D. W. Oldenburg, and J. Chen, 2014b, Where does the proppant go? Examing the application of electromagnetic methods for hydraulic fracture characterization: GeoConvention 2014 Expanded Abstracts, 1–7.

Hestenes, M. R., and E. Stiefel, 1952, Methods of conjugate gradients for solving linear systems: Journal of the National Bureau of Standards, 409–436.

Hibbs, A. D., 2014, Evaluation of deep subsurface resistivity imaging for hydrofracture monitoring: Technical report, GroundMetrics, Inc. (2nd quarterly report under US Department of Energy Contract DE–FE0013902).

House, L., 1987, Locating microearthquakes induced by hydraulic fracturing in crystalline rock: Geophysical Research Letters, **9**, 919–921. (doi:10.1029/GL014i009p00919).

Kriegshauser, B., O. Fanini, R. A. Mollison, L. Yu, T. Wang, and X. M. Tang, 2002, Method of using electrical and acoustic anisotropy measurements for fracture identification. (US Patent App. 10/317,457).

Pardo, D., and C. Torres-Verdín, 2012, Hydrofracture diagnosis in open-hole and steel-cased wells using borehole resistivity measurements: SEG Technical Program Expanded Abstracts, 1–6.

———, 2013, Sensitivity analysis for the appraisal of hydrofractures in horizontal wells with borehole resistivity measurements: Geophysics, **78**, D209–D222.

Pardo, D., C. Torres-Verdín, and M. Paszyznski, 2008a, Simulations of 3D DC borehole resistivity measurements with a goal–oriented *hp* finite-element method. Part II: through–casing resistivity instruments: Computational Geosciences, **12**, 83–89. (doi:10.1007/s10596-00709061-y).

Pardo, D., C. Torres-Verdín, and I. Z. Zhang, 2008b, Sensitivity study of borehole–to–surface and crosswell electromagnetic measurements acquired with energized steel casing to water displacement in hydrocarbon–bearing layers: Geophysics, **73**, F261–F268. (doi:10.1190/1.2993538).

Phillips, W. S., T. D. Fairbanks, J. T. Rutledge, and D. W. Anderson, 1998, Induced microearthquake patterns and oil–producing fracture systems in Austin Chalk: Tectonophysics, **289**, 153–169.

Polak, E., and G. Ribière, 1969, Note sur la convergence des méthodes de directions conjuguées: Revue Française d'Informatique Recherche Opérationnelle, **16**, 3543.

Pollastro, R. M., L. N. R. Roberts, and T. A. Cook, 2013, Geologic assessment of technically recoverable oil in the Devonian and Mississippian Bakken Formation, *in* Assessment of undiscovered oil and gas resources of the Williston Basin Province of North Dakota, Montana, and South Dakota, 2010 (ver. 1.1, November 2013): U.S. Geological Survey, Digital Data Series DDS69W, 5, 34.

Pribnow, D. F. C., C. Schütze, S. J. Hurter, C. Flechsig, and J. H. Sass, 2003, Fluid flow in the resurgent dome of Long Valley Caldera: implications from thermal data and deep electrical sounding: Journal of Volcanology and Geothermal Research, **127**, 329–345. (doi:10.1016/S0377-0273(03)00175-6).

Reeves, D. M., D. A. Benson, and M. M. Meerschaert, 2008a, Transport of conservative solutes in simulated fracture networks 1. Synthetic data generation: Water Resources Research, **44**, W05404. (doi:10.1029/2007WR006069).

Reeves, D. M., D. A. Benson, M. M. Meerschaert, and H. P. Scheffler, 2008b, Transport of conservative solutes in simulated fracture networks 2. Ensemble solute transport and the correspondence to operator-stable limit distributions: Water Resources Research, **44**, W05410. (doi:10.1029/2008WR006858).

Robinson, J., T. Johnson, and L. Slater, 2013, Evaluation of known-boundary and resistivity constraints for improving cross-borehole DC electrical resistivity imaging of discrete fractures: Geophysics, **78**, D115–127.

Rutledge, J. T., and W. S. Phillips, 2003, Hydraulic stimulation of natural fractures as revealed by induced microearthquakes, Carthage Cotton Valley gas field, east Texas: Geophysics, **68**, 441–442. (doi:10.1190/1.1567214).

Taftia, T. A., M. Sahimi, F. Aminzadeh, and C. G. Sammis, 2013, Use of microseismicity for determining the structure of the fracture network of large-scale porous media: Physical Review E, **87**, 032152. (doi:10.1103/PhysRevE.87.032152).

Tseng, H.-W., A. Becker, M. J. Wilt, and M. Deszcz-Pan, 1998, A borehole–to–surface electromagnetic survey: Geophysics, **63**, 1565–1572.

Weiss, C. J., 2001, A matrix–free approach to solving the fully 3D electromagnetic induction problem: SEG Technical Program Expanded Abstracts, **20**, 1451–1454.

Wills, P. B., D. C. DeMartini, H. J. Vinegar, J. Shlyapobersky,

W. F. Deeg, J. C. Woerpel, J. E. Fix, G. G. Sorrells, and R. G. Adair, 1992, Active and passive imaging of hydraulic fractures: The Leading Edge, **11**, 15–22.

Wilt, M., and M. Morea, 2004, 3d waterflood monitoring at Lost Hills with crosshole EM: The Leading Edge, **23**, 489–493.

Wright, P. M., S. H, Ward, H. P. Ross, and R. C. West, 1985, State-of-the-art geophysical exploration for geothermal resources: Geophysics, **50**, 2666–2699.

Yang, K., E. Celik, C. Torres-Verdín, and A. E. Yilmaz, 2013, Detection and quantification of 3D hydraulic fractures with multi–component low–frequency borehole resistivity measurements: SEG Technical Program Expanded Abstracts, 545–550.